energy&fuels

pubs.acs.org/EF Article

Torrefaction of *Acacia nilotica*: Oxygen Distribution and Carbon Densification Mechanism Based on In-Depth Analyses of Solid, Liquid, and Gaseous Products

Satyansh Singh, Jyoti Prasad Chakraborty,* and Monoj Kumar Mondal

Cite This: *Energy Fuels* 2020, 34, 12586−12597 Read Online

ACCESS | Metrics & More | Article Recommendations | Supporting Information

ABSTRACT: Torrefaction has been proven as a promising pretreatment process that can effectively reduce the moisture content and increase the energy density and higher heating value (HHV) of raw biomass and convert it into high-grade solid biofuel. To reveal the overall efficacy, mechanism, oxygen distribution, and carbon densification during torrefaction, in-depth analyses of solid residues, liquid condensates, and gaseous products became reasonably significant. Therefore, the present work aimed to establish the oxygen distribution and carbon densification mechanism during torrefaction by investigating the characteristics of solid residues, liquid condensates, and gaseous products by performing torrefaction between 225 and 300 °C and retention time (RT) (15−60 min). Results revealed that oxygen distribution and carbon densification are mainly responsible for the upgradation of raw biomass. The oxygen removal efficiency and carbon densification increased by 39.6 and 51.8%, respectively, at 300 °C and 30 min of RT. The densification of carbon in torrefied biomass resulted in an increase of HHV by 41.6% as compared to raw biomass. The oxygens distributed in the form of CO_2 (52.4 wt %) and CO (47.5 wt %) in gaseous products and oxygen-containing liquid condensates were mainly water (43.9 wt %) followed by phenols (18.0 wt %), ketones (15.6 wt %), furans (13.1 wt %), aldehydes (4.4 wt %), and acids (4.4 wt %) at 300 °C and 30 min of RT. The physical property like water content improved due to dehydration reaction, while viscosity and pH improved due to decrease in water content and acidic compounds, respectively, present in the liquid condensate. The ^{13}C NMR spectroscopy suggested that the total aromatic carbon and aromaticity of the liquid condensate increased with temperature during the process.

1. INTRODUCTION

Biomass, as a vital source of renewable energy,[1−3] has a huge prospective to be transformed into biofuels, bio-based materials,[4] and various value-added chemicals.[5] Various biomass sources include forest and agricultural residue, wood waste from milling industries, and specially planted energy crops such as switchgrass or prairie perennials.[6−8] *Acacia nilotica* (Prickly Acacia), a type of forest tree native to Australia, Africa, and Madagascar,[9] is readily available in Southeast Asian and African countries. It is suited for planting on waste, barren, and marginal lands having low productivity and can survive in both droughts and flooded conditions. In India, the wood (167 tons per hectare) as well as pod (0.6 million tons per year) production of *A. nilotica* is very high.[10]

Regardless of many advantages such as large availability, easy accessibility, lower emission of SO_x and NOx with respect to coal, as well as carbon neutrality, biomass is associated with many challenging characteristics such as higher moisture and oxygen contents, low energy density, large affinity to water, higher grinding energy, biodegradable, and complex and heterogeneous structure.[11−14] These characteristics have an adverse impact on the energetic utilization of biomass for bioenergy and value-added chemicals by decreasing the efficiency of the process and increasing the transportation and handling costs.[15,16] Nevertheless, biomass might be a potential source of renewable and clean energy by deploying appropriate pretreatment techniques to enhance its quality. Torrefaction has been ascertained as a capable pretreatment technique that can upgrade the quality, such as higher moisture and oxygen contents, low energy density, large affinity to water, higher grinding energy, biodegradable, complex, and heterogeneous structure of biomass. Torrefaction may be defined as a thermochemical pretreatment process that occurs between 200 and 300 °C under normal pressure and an inert atmosphere with a low heating rate and retention time.[17−22]

The three major components of biomass are hemicellulose, cellulose, and lignin. They account for 20−40, 40−60, and 10−25 wt %, respectively, of the total lignocellulosic biomass.[23] The temperature ranges for thermal degradation of hemicellulose, cellulose, and lignin are 220−315, 315−400, and 160−900 °C, respectively.[23] Hence, the thermal degradation behavior of biomass depends on the quantities of hemicellulose, cellulose, and lignin present in the biomass. It is important to mention that torrefaction is also called a mild pyrolysis process. Thus, the reaction pathway followed during torrefaction of biomass would be similar to pyrolysis of biomass; however, distribution of products will be different,

Received: May 25, 2020
Revised: August 30, 2020
Published: August 31, 2020

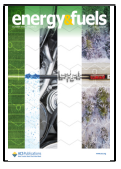

https://dx.doi.org/10.1021/acs.energyfuels.0c01673
Energy Fuels 2020, 34, 12586−12597

since those products that are formed at a higher temperature will not be identified during torrefaction. Hemicellulose consists of a short chain of heteropolysaccharides, which provides a branched structure to the biomass.[24] The monosaccharide units of hemicellulose are mainly hexoses and pentose.[25] Hemicellulose of hardwood mainly contains xylose and galactose monomeric units. Hemicellulose, being the least thermally stable component of biomass, degrades at a much faster rate than cellulose and lignin during thermal decomposition.

The products from torrefaction contain solid residues (torrefied biomass), liquid condensates, and noncondensable gases.[26] The efficacy of torrefied biomass as a superior fuel to raw biomass has been extensively explored by researchers because torrefaction can produce torrefied biomass having a lower moisture content, higher energy density, and lower oxygen and hydrogen contents.[27] These improved characteristics of torrefied biomass contributed to the improvement of both fuel and logistic properties. For instance, Grams et al.[7] investigated the surface characteristics of biomass after torrefaction and reported that the rupture of the biomass surface takes place after torrefaction. Chen et al.[28] performed the torrefaction of bamboo chips to upgrade them as good-quality solid biofuels. Morales et al.[29] studied the effect of severity of torrefaction on flow characteristics of biomass and reported that with an increase in temperature, finer, rounder, and more regular particles having better flow properties were obtained. Kanwal et al.[30] studied the physicochemical characteristics of sugarcane bagasse and found that torrefaction improves the quality of sugarcane bagasse in terms of better grindability, hydrophobicity, and higher heating value (HHV). In the published literature, a relatively small number of articles have been reported about characteristics of liquid condensates and gases released from torrefaction. Chen et al.[31] performed torrefaction of hemicellulose, cellulose, and lignin individually to study the properties of solid residues, liquid condensates as well as gaseous products. Ma et al.[32] studied torrefaction of lignin and reported that G-type and P-type phenolic compounds were dominant in the liquid condensate, and CO_2 was mainly present in gaseous products. Prins et al.[33] conducted the torrefaction of deciduous and coniferous wood and found that the former gives more methanol and acetic acid. Chen et al.[34] carried out the torrefaction of rice husk and found that the energy yield of gaseous and liquid condensates increased on increasing the temperature. Chen et al.[19] investigated the properties of liquid condensate and gas from torrefaction. They also reported that liquid condensates mainly consisted of alcohol, acids, ketones, aldehydes, etc.

The decrease in oxygen content (deoxygenation) and an increase in carbon content (carbon densification) after torrefaction are mainly responsible for the upgradation of biomass.[35,36] There are mainly two ways to decrease the oxygen content from biomass during torrefaction: (1) in the form of gaseous products such as CO_2 and CO, and (2) due to dehydration reaction during torrefaction. It was found that the release of gaseous products contributed faster than dehydration toward the removal of oxygen from biomass during torrefaction.[37−39] Thus, it is of prime importance to establish the oxygen migration and carbon densification mechanism of torrefaction. This involves the characteristics of solid residues, liquid condensates, and gaseous products.[40]

However, most of the works published on torrefaction are related to characteristics of solid products such as proximate and ultimate analyses, surface morphology, chemical and compositional analyses with the variation of temperature, retention time, heating rate, particle size, reactor environment, etc.[7,27−30] In fact, the combined study of solid residues, liquid condensates, and gaseous products and the mechanism of oxygen migration and carbon densification have rarely been investigated. The liquid condensates and gaseous products contribute to 10−50 wt % of the total product from torrefaction depending on the process parameters.[26] Hence, the significance of liquid condensates and gaseous products cannot be overlooked. Also, the decreased oxygen content in torrefied biomass during torrefaction transferred to liquid condensates and gaseous products. Thus, oxygen distribution and the carbon densification mechanism cannot be understood without analysis of liquid and gaseous products.

Therefore, the present work aimed to establish the oxygen distribution and carbon densification mechanism during torrefaction by investigating the characteristics of solid residues, liquid condensates, and gaseous products by performing torrefaction between 225 and 300 °C and retention time (RT) (15−60 min). Solid products were subjected to proximate, ultimate, and thermogravimetric analyses (TGA), Fourier transform infrared (FTIR) analysis, and X-ray diffraction (XRD) analysis for their physicochemical characteristics. The properties of liquid condensates were studied using FTIR, ^{13}C NMR spectroscopy, and gas chromatography−mass spectrometry (GC−MS) analyses. The quality and quantity of gaseous products were investigated using gas chromatography (GC−TCD). In addition, properties of liquid condensates like higher heating value (HHV), viscosity, pH, density, carbon residue, and ash content were also examined. Finally, based on the characteristics of solid residues, liquid condensates, and noncondensable gaseous products, the mechanism of oxygen distribution and carbon densification was suggested.

2. MATERIALS AND METHODS

2.1. Material. In this study, *A. nilotica* collected from a village situated near Banaras Hindu University, Varanasi (latitude: 25.582208; longitude: 82.868677), was chosen as a raw material. After collection, biomass was exposed to sunlight to remove moisture from the surface. A cutting mill (Retsch model SM 300, Germany) was employed for cutting the biomass into fine particles. The particles between 0.7 and 1.25 mm size were selected for experiments. After that, they were placed inside a hot air oven at 80 °C for 24 h to remove moisture and attain constant weight before carrying out experiments. In this work, the dried *A. nilotica* is indicated as RAW, *A. nilotica* obtained after torrefaction is indicated as T-*X*-*Y*, and liquid condensate is marked as TO-*X*-*Y*, where variables *X* and *Y* denote temperature and retention time, respectively, during the process. For instance, T-250-30 indicates torrefied *A. nilotica* found at 250 °C and 30 min retention time, and TO-250-30 denotes liquid condensate obtained at 250 °C and 30 min retention time.

2.2. Experimental Procedure for Torrefaction and Material Balance. Torrefaction experiments were performed in a vertical quartz reactor. The diameter and length of the reactor were 2.5 and 80 cm, respectively. The reactor was heated externally by a split tube furnace (NSW-104, New Delhi) having a single heating zone of length 15 cm.[10,41,42] Temperature, retention time, and heating rate of the furnace were controlled by a proportional-integral-derivative (PID) controller attached to the furnace. A K-type thermocouple was inserted into the reactor for measuring the temperature of the biomass. The thermocouple was placed in the reactor such that it only touches the upper surface of the loaded biomass sample. Ceramic wool was placed at the notches inside the reactor as a support for the biomass sample. A countercurrent condenser was connected to the bottom of the reactor, and it was connected to a recirculating bath

https://dx.doi.org/10.1021/acs.energyfuels.0c01673
Energy Fuels 2020, 34, 12586−12597

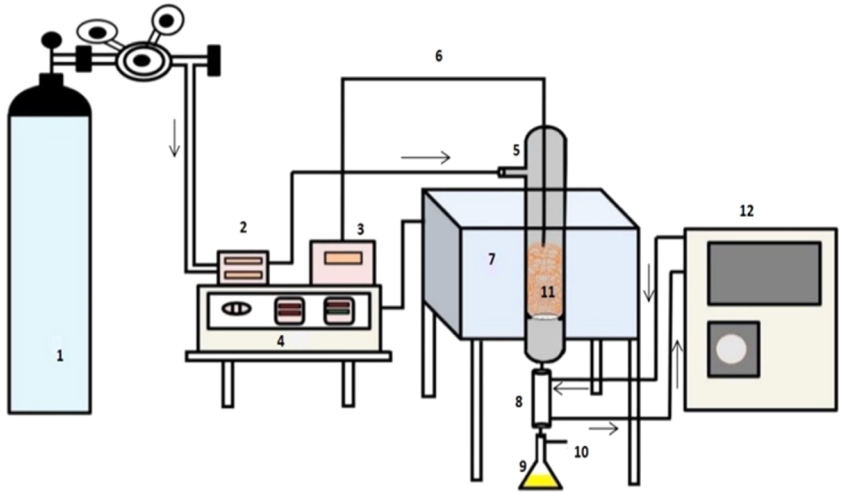

Figure 1. Schematic diagram of the experimental setup: (1) nitrogen cylinder, (2) mass flow controller, (3) temperature measuring unit, (4) split tube furnace (NSW-104) controller, (5) long tube fixed-bed reactor, (6) K-type thermocouple, (7) split tube furnace (NSW-104), (8) condenser, (9) oil collector, (10) gas collection, (11) biomass with ceramic wool bed gas collector, and (12) chiller (Eyela CA-1112CE).[41]

(Eyela CA-1112CE, Japan) for condensing the condensable gaseous products. The temperature of the recirculating bath was maintained at −5 ± 2 °C. The liquid condensate was collected in a filtering bolt neck tabulation flask connected at the bottom of the condenser. Initially, nitrogen gas was passed through the reactor for 45 min and maintained throughout the experiment to maintain the inert atmosphere inside the reactor. The flow rate of nitrogen gas (45 mL/min) was maintained using a mass flow controller (Bronkhorst, The Netherlands). The schematic diagram of the experimental setup is shown in Figure 1[41] In each experimental run, 6 g of biomass was loaded into the reactor. The torrefaction of biomass was carried out at 225, 250, 275, and 300 °C with retention times of 15, 30, 45, and 60 min, in each case, respectively, and at a constant heating rate of 15 °C/min. As soon as the heating of the furnace was turned on, the temperature of the biomass inside the reactor started increasing from atmospheric temperature (around 27 °C) to a set point temperature (for example, 300 °C) as measured by a K-type thermocouple (initially, the thermocouple temperature lacked behind the controller temperature by 10 °C; however, it reaches the controller temperature after a certain time). Then, the set point temperature was maintained for retention time (for example, 60 min) set in the control panel of the furnace. After the completion of retention time, the heating of the furnace stops automatically and the self-cooling of the furnace starts. The reactor system was disassembled after the room temperature was attained. The torrefied biomass and liquid condensate were collected for further analysis. The gaseous products were collected in a Tedlar bag during the experiments. The experimentations were conducted in duplicate, and the mean values were mentioned to confirm the reproducibility of results.

For material balance, the torrefied biomass was collected and weighed when the reactor attained room temperature. The liquid condensate was collected in a filtering bolt neck tabulation flask. For gaseous products, it was assumed that no gas (noncondensable) is formed below 200 °C. When the temperature of the thermocouple reached 200 °C during heating, the gas sample was taken at a regular interval of 25 °C until it reaches the desired torrefaction temperature. During the constant temperature zone, samples were collected at regular intervals. The permanent gases were collected in the Tedlar bag at regular intervals of time connected to the opening of the filtering bolt neck tabulation flask. The gaseous samples were taken from the Tedlar bag for gas chromatography analysis. For removal of any oxygen trapped inside the conical flask, the reactor setup was purged with nitrogen gas for 45 min before the heating of the furnace was turned on. The Tedlar bag was connected to the flask as soon as the heating of the furnace was turned on. Moreover, samples were also collected during the cooling phase down to a temperature of 200 °C. The total durations of heating (from 200 °C to T_{torr}), constant temperature zone, and cooling (T_{torr} to 200 °C) were noted using a stopwatch during cooling. The retention time may vary during the experiment; accordingly, the interval of sampling can be varied. The gas sample was analyzed in gas chromatography (GC−TCD). The detailed procedure for calculation of the mass of noncondensable gases and GC−TCD has been given in procedures S1 and S2 (Supporting Information).

The yields of solid residues, liquid condensates, and gaseous products were calculated using eqs 1−3.

$$\text{solid yield (wt \%) (SY)} = \frac{\text{wt of torrefied biomass (g)}}{\text{wt of raw biomass (g)}} \times 100 \quad (1)$$

$$\text{liquid yield(wt \%) (LY)} = \frac{\text{wt of liquid condensate (g)}}{\text{wt of raw biomass (g)}} \times 100 \quad (2)$$

$$\text{gas yield (wt \%) (GY)} = \frac{\text{wt of gaseous product (g)}}{\text{wt of raw biomass (g)}} \times 100 \quad (3)$$

Energy yield (EY) of the solid residue was calculated as follows:

$$\text{energy yield(EY)} = (\text{SY})\frac{\text{HHV}_{\text{db, torrefied biomass}}}{\text{HHV}_{\text{db, raw biomass}}} \quad (4)$$

2.3. Methods Used for Characterization of Raw Biomass and Products of Torrefaction. The proximate and elemental analyses and HHV of raw and torrefied biomass were performed. Details about the standard protocols have been mentioned in procedure S2 (Supporting Information). The compositions of raw and torrefied biomass were studied by following the method enumerated by Bledzki et al.[43] Details of the method have been given in Figure S1 (Supporting Information). The thermal behaviors of raw and torrefied biomass were investigated using TGA (Perkin Elmer STA 6000). The FTIR analyzer (Varian 1000) was used to reveal the chemical functional groups presenting raw and torrefied biomass as well as liquid condensates. The crystalline behavior of raw and torrefied biomass was studied by an X-ray diffractometer (XRD, model Mini Flux II, Rigaku, Japan). The physical properties of liquid condensates obtained at different conditions were estimated. The density of liquid condensates was calculated by following the procedure of the ASTM D1298 standard. Carbon residue of liquid condensates was determined using the Ramsbottom carbon residue apparatus (IP 14/65). The standard protocol ASTM D1744 was employed for measurement of water content in liquid condensates by

https://dx.doi.org/10.1021/acs.energyfuels.0c01673
Energy Fuels 2020, 34, 12586−12597

employing the Karl Fischer titrator (ESICO, μP KARL FISCHER moisture titrator, Ambala, India). The Brookfield digital viscometer (LVDV-II+Pro) was employed for measuring the density of liquid condensates. The chemical composition of liquid condensates obtained after torrefaction was determined using a GC−MS (TURBOMASS\GBPIC GCMS.PRO) analyzer. The distribution of different types of carbon in liquid condensates was enumerated by employing ^{13}C NMR spectrometry. Details about the characterization such as TGA, FTIR, XRD, GC−MS, and ^{13}C NMR are given in procedure S2.

3. RESULTS AND DISCUSSION

3.1. Product Yield and Material Balance. The distributions of solid residues, liquid condensates, and gaseous products at different temperatures and retention times are shown in Figures 2 and S2. The heating rate was kept constant at 15 °C/min. The mass balance was calculated using the procedure discussed in the Supporting Information (Procedure S1) to verify the reliability of the experimental procedure. There were 16 sets of experiments, and in most of the cases, the sum of solid residues, liquid condensates, and gaseous yields was greater than 96%, while in some cases, it was 92%. This difference between totalities of yield might be due to the problems of collecting the products completely and also due to some experimental inaccuracy.[34] The experimental inaccuracies in K-type thermocouples for temperature measurement and heating rate measurement were observed to be ±1.1 and ±0.15 °C/min, respectively. No inaccuracy was observed during the measurement of retention time.

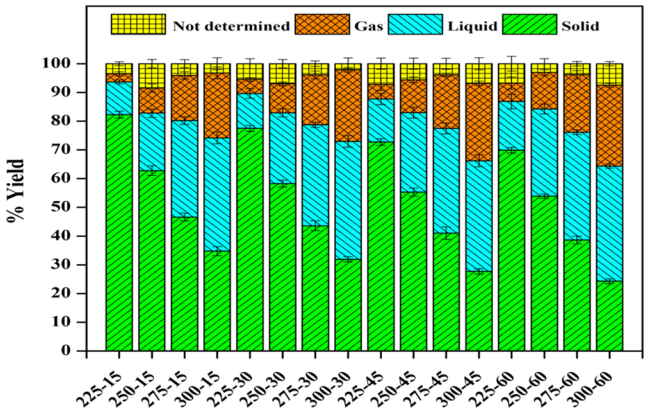

Figure 2. Profiles of product yield with the variation of temperature.

The product yield mainly depends on parameters like temperature and retention time. The solid yield gradually decreases as the temperature and retention time increase during the process due to the increase in the rate of devolatilization and intense water loss.[31,33] On the other hand, liquid condensate and gas yields increase with the increase in temperature and retention time. It was noticed that the effect of temperature on product yield was more pronounced than that of retention time. For example, at a particular retention time (30 min), the yields of solid, liquid, and gas products varied within 66.9−39.5, 17.1−31.1, and 15.8−29.2%, respectively, when the temperature was varied from 225 to 300 °C. However, at a particular temperature (250 °C), yields of solid residues, liquid condensates, and gas products varied within 63.9−54.7, 18.9−27.0, and 17.0−18.1%, respectively, when the retention time was varied from 15 to 60 min. Sharp changes can be seen in the case of temperature variation, while uniform variation was observed in the case of retention variation (Figures 2 and S2). A similar trend in results was obtained by Chen et al.,[34] Han et al.,[20] and Prins et al.[33] Hence, significant variation in the characteristics of products may not be observed when the retention time was varied. Keeping this in mind, solid and liquid condensates obtained at different temperatures (225, 250, 275, 300 °C) and a fixed retention time of 30 min were taken for further characterization.

3.2. Characteristics of Solid Products. *3.2.1. Proximate and Ultimate Analyses, Energy Yield, and Compositional Analysis.* Table 1 represents the results of proximate and ultimate analyses of raw[41] and torrefied biomass. It was found that the temperature showed a prominent impact on moisture content, ash content, volatile matter, and fixed carbon. Moisture content and volatile matter both decreased, whereas fixed carbon and ash content increased as the temperature increased during torrefaction. The moisture contents of raw

Table 1. Physicochemical Characteristics and Fiber Analyses of Raw[41] and Torrefied Biomasses

analysis	raw	T-225-30	T-250-30	T-275-30	T-300-30
		Proximate Analysis (wt %)			
moisture content	6.4 ± 0.42[a]	3.1 ± 0.12	1.6 ± 0.09	1.3 ± 0.05	0.5 ± 0.01
ash content	0.7 ± 0.19	1.5 ± 0.01	2.0 ± 0.01	2.1 ± 0.01	2.3 ± 0.28
volatile matter	79.0 ± 1.80	58.4 ± 2.99	44.8 ± 2.09	41.5 ± 0.21	38.8 ± 0.02
fixed carbon[b]	13.9 ± 0.91	37 ± 1.48	51.6 ± 2.16	55.1 ± 2.92	58.4 ± 2.92
		Ultimate Analysis (wt %)			
C	43.6 ± 0.77	52.2 ± 0.02	57.5 ± 2.88	60.6 ± 0.67	66.3 ± 0.27
H	7.5 ± 0.77	5.1 ± 0.88	3.0 ± 0.11	2.8 ± 0.07	2.1 ± 0.07
O[b]	48.5 ± 0.73	41.3 ± 0.37	37.6 ± 0.15	34.6 ± 0.08	29.3 ± 0.86
N	0.4 ± 0.15	1.4 ± 0.01	1.9 ± 0.01	2.0 ± 0.01	2.3 ± 0.02
S	BDL	BDL	BDL	BDL	BDL
HHV (MJ/kg)	18.6 ± 0.72	20.8 ± 0.50	21.8 ± 0.42	24.3 ± 0.18	26.4 ± 0.42
energy yield (solid product)(%)		75.3	74.2	59.6	55.2
		Fiber Analysis (wt %)			
hemicellulose	28.6 ± 0.95	23.7 ± 1.01	16.6 ± 1.20	12.7 ± 1.30	3.7 ± 0.88
cellulose	41.6 ± 0.90	44.5 ± 0.98	40.8 ± 0.87	37.4 ± 1.09	30.8 ± 1.22
lignin	24.2 ± 0.43	27.9 ± 1.12	37.3 ± 1.55	45.9 ± 1.39	59.9 ± 2.44

[a]Standard deviation. [b]Calculated by difference; BDL, below the detection limit.

https://dx.doi.org/10.1021/acs.energyfuels.0c01673
Energy Fuels 2020, 34, 12586−12597

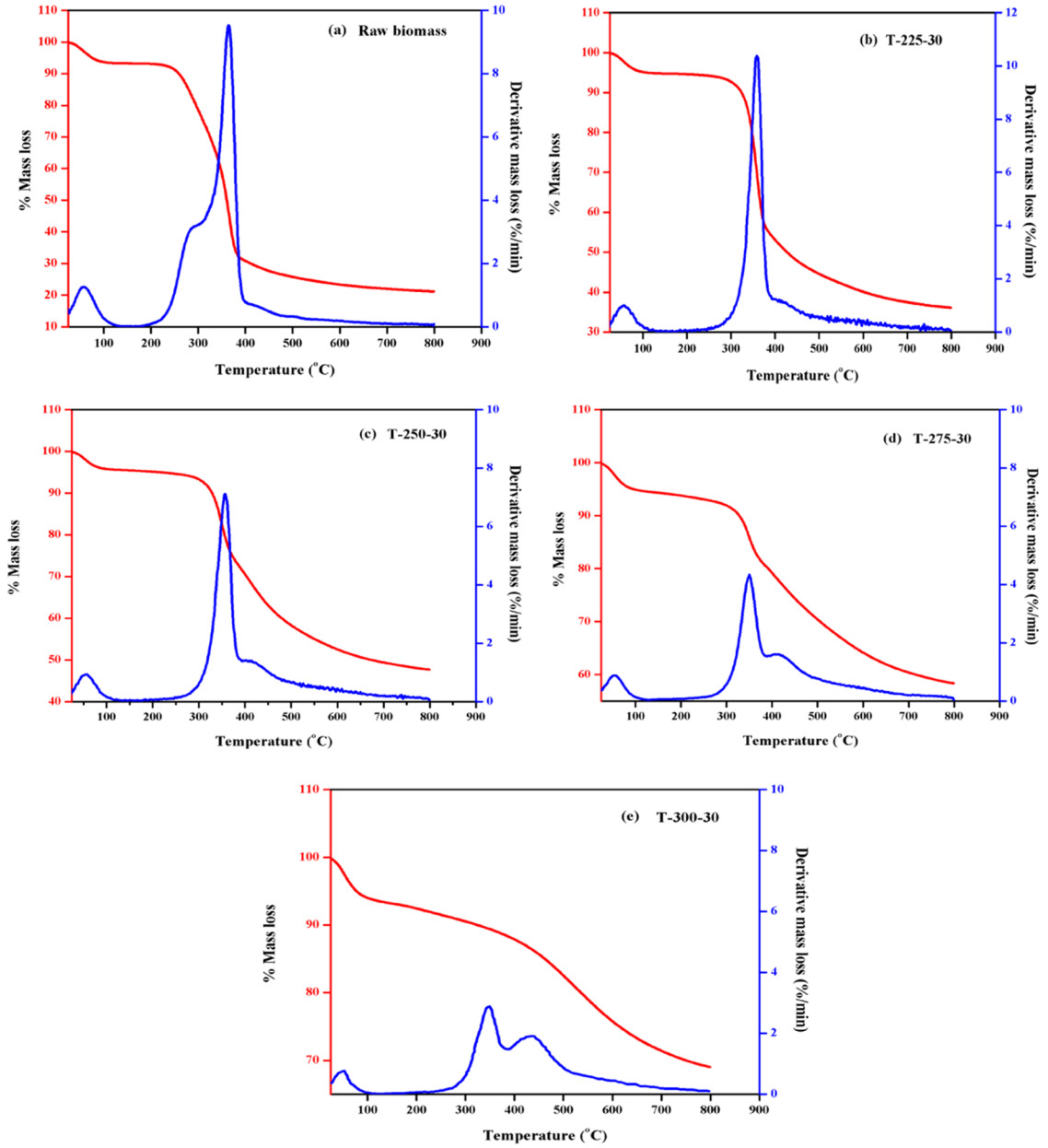

Figure 3. Thermogravimetric analysis at different temperatures and 30 min retention time: (a) raw biomass,[41] (b) T-225-30, (c) T-250-30, (d) T-275-30, and (e) T-300-30.

biomass, T-225-30, T-250-30, T-275-30, and T-300-30 were found to be 6.4, 3.1, 1.6, 1.3, and 0.5%, respectively. Thus, the moisture content was reduced by 92.1% when the temperature increased from 225 to 300 °C. The volatile matters of raw biomass, T-225-30, T-250-30, T-275-30, and T-300-30 were found to be 79.0, 58.4, 44.8, 41.5, and 38.8%, respectively. A decrease of 50.8% was observed in the case of volatile matter. The fixed carbon contents of raw biomass, T-225-30, T-250-30, T-275-30, and T-300-30 were found to be 13.9, 37, 51.6, 55.1, and 58.4%, respectively. Consequently, the fixed carbon content was increased by 4.2 times compared to the raw biomass. Also, the ash contents of raw biomass, T-225-30, T-250-30, T-275-30, and T-300-30 were found to be 0.7, 1.5, 2.0, 2.1, and 2.3%, respectively. Accordingly, the ash content increased by approximately three times compared to the raw biomass. The rise in temperature results in a relative decrease in the moisture content and volatile matter and a relative increase in the fixed carbon and ash contents of biomass as the devolatilization reaction increases.[44]

The result of the ultimate analysis can be explained more conveniently through the van Krevelen diagram (Figure S3). This diagram depicts the profile of the atomic ratio of H/C versus the atomic ratio of O/C.[19] For raw biomass, both H/C and O/C atomic ratios were found to be 0.17 and 1.10, respectively. However, for torrefied biomass, both the ratios decreased markedly, as shown in Figure S3. Thus, in torrefaction, the release of hydrogen and oxygen is more prominent as compared to carbon.

Energy yield (EY) denotes the amount of energy conserved in the biomass after torrefaction. EY is a function of product yield and its higher heating value. The EY of torrefied biomass decreased with temperature and retention time. As the temperature and retention time increase, dehydrogenation and deoxygenation of biomass become more prominent.

https://dx.doi.org/10.1021/acs.energyfuels.0c01673
Energy Fuels 2020, 34, 12586−12597

Additionally, at higher retention time, exposure of biomass for the reaction is larger; the reaction takes place for a longer time, favoring the devolatilization reaction.[18] Consequently, solid yield decreases with a relative increase in liquid condensates and gaseous products. EYs for T-225-30, T-250-30, T-275-30, and T-300-30 were found to be 75.3, 74.2, 59.6, and 55.2%, respectively. It shows that the differences between EY from 225 to 250 °C and from 275 to 300 °C are not pronounced. However, between 250 and 275 °C, the difference is significant. A similar trend regarding EY was also noticed for bamboo and oil palm fiber pellets by Chen et al.[18,19]

The fiber contents of raw biomass, T-225-30, T-250-30, T-275-30, and T-300-30 are mentioned in Table 1. Hemicellulose, cellulose, and lignin for raw biomass were found to be 28.6, 41.6, and 24.2%, respectively. In the course of torrefaction, as the temperature increases from 225 to 300 °C, a noticeable decline in hemicellulose (28.6−3.7 wt %) was perceived. The degradation of hemicellulose leads to the formation of gaseous products like CO_2, CO, and various oxygen-containing compounds along with H_2O in the liquid condensate. Similar results have been reported by many researchers.[34,45,46] However, the relative cellulose content initially increased, in the case of low-temperature torrefaction (T-225-30 and T-250-30), and then decreased by 25.9% with respect to raw biomass when the temperature was increased to 300 °C. At lower temperatures, a significant amount of hemicellulose degraded, while most of the cellulose remained intact with biomass. The overall decrease in cellulose content attributed to the carbonization reaction of biomass, which is responsible for the higher fixed carbon content of torrefied biomass, is presented in Table 1. The thermal stability of lignin is the highest among the components of biomass, and it degrades in a wide range of temperatures. Thus, the relative lignin content of torrefied biomass is higher than that of raw biomass. Consequently, a 59.6% increase in lignin content was noticed when the temperature increased from 225 to 300 °C. Moreover, Chen et al.[34] also mentioned that the carbonization of hemicellulose and cellulose contents resulted in relatively higher lignin contents. Therefore, it can be concluded that during torrefaction, the breakdown of hemicellulose is more prominent than cellulose and lignin.

3.2.2. Thermal Behavior of Torrefied Biomass. The thermogravimetric analyses of raw[41] and torrefied biomass are shown in Figure 3a−e. From the TGA curve, it can be observed that mass loss for raw biomass is the highest, while it is the lowest for T-300-30. This is due to the presence of highest amount of volatile matter in raw biomass and lowest amount for T-300-30, respectively. These results comply with the results presented in Table 1. During pyrolysis, residual char yield is the highest for T-300-30, while raw biomass yields the least residual char. In the case of raw biomass, the devolatilization process begins at about 220 °C and continues quickly with an increase in temperature up to about 400 °C. From Figure 3b−e, it can be observed that the range of temperatures for devolatilization shrinks for torrefied biomass, and the degree of shrinkage increased with an increase in process temperature. In the case of the DTG curve, temperatures less than 100 °C can be attributed to the removal of surface moisture from raw and torrefied biomass during pyrolysis. It can be seen that the intensity of peaks corresponding to moisture removal is the maximum for raw biomass and gradually decreases for torrefied biomass obtained at a higher temperature. The moisture content in torrefied biomass is lower than that in the raw biomass, as presented in Table 1. The shoulder seen in the DTG profile signifies the degradation of hemicellulose of the biomass. For raw biomass, usually, these shoulders were noticed at around 300 °C.[23,47] Comparable shoulders appeared for raw biomass (Figure 3a). However, for torrefied biomass, the shoulder was wiped out, confirming that hemicellulose is previously decomposed in the course of torrefaction. The peaks at a maximum mass loss in the DTG profile are related to cellulose.[23] The peaks related to cellulose for raw and torrefied biomass appeared at 358 °C. Comparing raw and torrefied biomass, the obvious decrease in intensity of cellulose peaks for T-250-30, T-275-30, and T-300-30 compared to the raw biomass is due to degradation of cellulose up to this temperature. However, in the case of T-225-30, the cellulose peak intensity is slightly higher than the raw biomass. At 225 °C, primarily hemicellulose decomposition takes place, consequently increasing the relative amount of cellulose in the torrefied biomass obtained after torrefaction at 225 °C.

3.2.3. Fourier Transform Infrared Spectroscopy of Solid Residues and Liquid Condensates. The FTIR analysis was executed to investigate the structural modifications of functional groups associated with raw[27] and torrefied biomass as well as liquid condensates. The results are shown in Figure 4a,b. Between 200 and 300 °C, major mass loss in biomass occurred due to the breakdown of hemicellulose and the fractional decomposition of cellulose and lignin. Consequently,

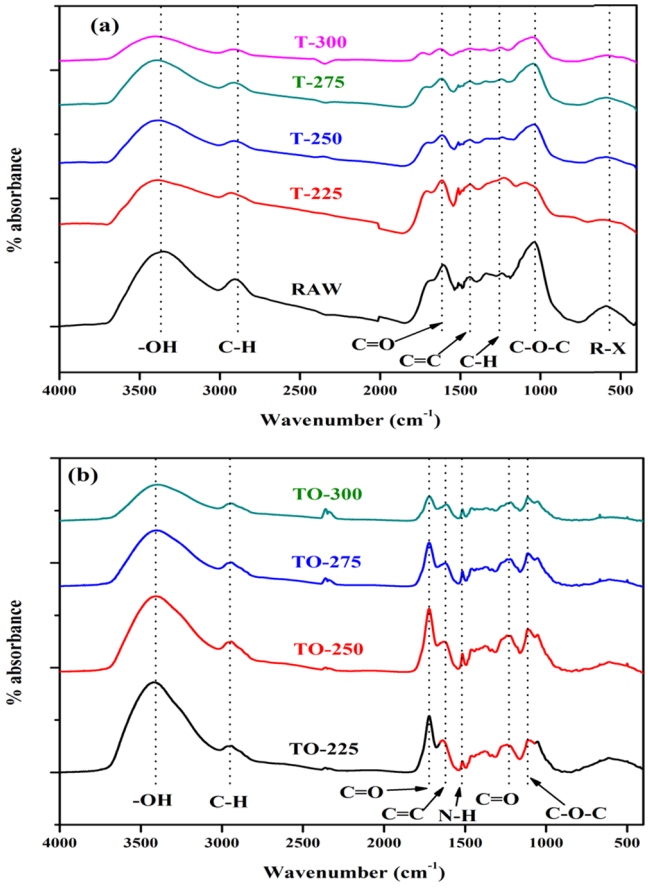

Figure 4. FTIR analyses of raw,[27] torrefied biomass, and liquid condensates obtained at different temperatures and 30 min retention time. (a) Raw and torrefied biomass and (b) liquid condensates.

https://dx.doi.org/10.1021/acs.energyfuels.0c01673
Energy Fuels 2020, 34, 12586−12597

a structural and chemical modification associated with biomass is attributed to the hemicellulose decomposition mainly. Major peaks in the ranges 3500−3100 cm^{-1}, 2950−2750 cm^{-1}, 1700−1500 cm^{-1}, and 1200−1000 cm^{-1} were detected as a result of stretching vibration in the O−H bond, C−H bond, (C═O bond, C═C bond, and N−H bond), and C−O−C bond, respectively.[48−50] The decrease in intensity between the 3500 and 3100 cm^{-1} waveband can be ascribed to the cleavage of hydroxyl groups associated with the biomass. Reduction in peak intensity between 1700 and 1500 cm^{-1} might be due to the cleavage of ester bonds present in hemicellulose.[51] The vibration associated with C−H stretching and distortion in the wavebands of 2926−2855 and 1462−1362 cm^{-1}, individually, indicates the presence of an alkane group in the raw and torrefied biomass. The absorption bands between 1420−1610 and 690−900 cm^{-1} can be attributed to the occurrence of monocyclic, polycyclic, and substituted aromatic compounds.[52] Similar wavebands were also observed in the present study. As the severity of torrefaction increases, the height of peaks reduces in the cases of torrefied T-225-30, T-250-30, T-275-30, and T-300-30, which complies with the structural and chemical modification of the biomass. Also, a severe condition of torrefaction, peaks associated with different functional groups shifted toward a lower wavenumber.[30] Comparing the FTIR analyses of solid residues and liquid condensates (Figure 4a,b) from torrefaction, the intensities of −OH and C═O peaks are slightly higher in the case of liquid condensates than the solid product. This might be due to the condensation and hydroxylation reaction for the −OH bond and the presence of ketones in the liquid condensates for the C═O bond. The variation in peak intensity for different torrefied biomass and liquid condensates revealed that the chemical composition of products varies with the process variable, such as temperature.

3.2.4. X-ray Diffraction (XRD) Analysis. XRD analyses were done to observe the effect of torrefaction on the crystallinity of raw[27] and torrefied biomass. Among the three major constituents of biomass (cellulose, hemicellulose, and lignin), cellulose may show an amorphous or crystalline behavior, while hemicellulose and lignin show amorphous character.[39,53,54] Also, the thermal stability of crystalline cellulose is higher than amorphous cellulose since the former has a higher cohesion energy density.[39] The broad peaks observed at a 2θ value at around 16 and 22° for raw biomass represent 101 and 002 lattice spacings in cellulose in woody biomass.[55] In the case of T-225-30, both peaks become slightly narrower, suggesting the increase in crystallinity. However, with the increase in severity during torrefaction, both peaks become wider, and the peak intensity also decreases, suggesting a decrease in the crystallinity of torrefied biomass at a higher temperature. The results are shown in Figure 5. The CrI values for raw, T-225-30, T-250-30, T-275-30, and T-300-30 were found to be 44.97, 51.31, 42.41, 35.48, and 21.64, respectively. The CrI depends on the competitive decomposition of crystalline and amorphous cellulose.[39] The obvious decrease in CrI for T-250-30, T-275-30, and T-300-30, in comparison to raw biomass, is attributed to the decomposition of cellulose at a higher temperature and release of a small amount of CO_2 and H_2O from the biomass during torrefaction.[39] However, in the case of T-225-30, the CrI is higher than the raw biomass. This might be attributable to a major breakdown of hemicellulose and a relative increase in cellulose content up to 225 °C of torrefaction. In addition, this increase in CrI might be due to the recrystallization of amorphous cellulose up to 225 °C.[39,54]

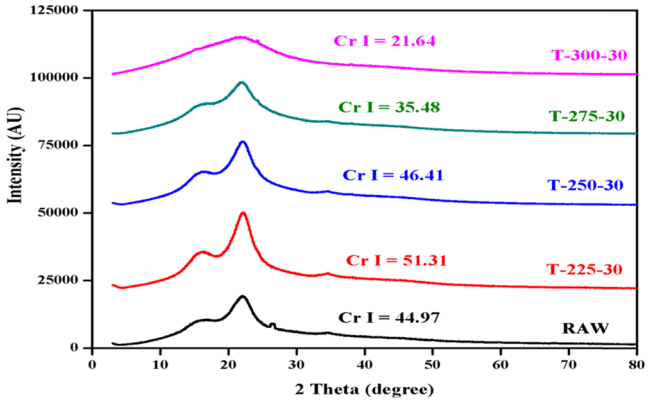

Figure 5. XRD analyses of raw[27] and torrefied biomasses.

3.3. Characteristics of Gaseous Products. Figure 6 shows the variation in the composition of gases at different temperatures and retention times during torrefaction. The major components of gases are CO_2 and CO; however, traces of H_2 and CH_4 were also found at higher temperatures. It was found that the composition of the gaseous product was highly influenced by temperature (Figure 6), while retention time had minimal impact. For example, at a particular retention time (60 min), the mass percentages of CO_2, CO, H_2, and CH_4 varied in the ranges 75.3−49.8, 24.1−46.0, 0.5−1.9, and 0−2.0%, respectively, as the temperature varied from 225 to 300 °C. However, at a particular temperature (300 °C), the mass percentages of CO_2, CO, H_2, and CH_4 varied in the ranges 52.2−49.8, 44.6−46.0, 1.7−1.9, and 1.4−2.0%, respectively, as the retention time varied from 15 to 60 min. At a lower temperature (225 °C), CO_2 and CO were the main gaseous products, while CH_4 was not detected up to 275 °C. With the increase in temperature, the fraction of CO_2 decreased, while the fractions of CO and H_2 increased. The result complies with the published literature.[16,20,33,34]

3.4. Characteristics of Liquid Condensates. *3.4.1. Physical Characteristics of Liquid Condensates.* The physical properties of liquid condensates are mentioned in Table 2. The liquid condensate has a light-brown color at a lower temperature, while the color deepens and becomes dark brown under severe torrefaction conditions. The water contents determined from the Karl Fischer titrator were found to be 65, 58, 52, and 45 wt % of the liquid condensate for TO-225-30, TO-250-30, TO-275-30, and TO-300-30, respectively. With an increase in temperature, the decrease in water content is attributed to the intense reaction of water molecules with volatile matter and torrefied biomass.[19] Accordingly, less water was found in liquid condensates at a higher temperature during torrefaction. The HHVs of liquid condensates TO-225-30, TO-250-30, TO-275-30, and TO-300-30 were found to be 10.2, 12.5, 13.4, and 14.3 MJ/kg, respectively. Usually, the HHV of bio-oil obtained from pyrolysis is 17 MJ/kg.[19] Thus, the HHV of liquid condensate from torrefaction is lower than that from the bio-oil from pyrolysis. Since the amount of water in the torrefied liquid condensate is quite high, significant energy is consumed in the evaporation of this water content. As suggested by Chen et al.,[19] the dewatering of liquid condensate from torrefaction can enhance the higher heating value, and it can be used as a fuel. The density and viscosity of liquid are properties that are associated with the flow behavior of a liquid. Density and viscosity vary from 1052 to 1086 kg/m^3 and from 0.9 to 3.8 c,

https://dx.doi.org/10.1021/acs.energyfuels.0c01673
Energy Fuels 2020, 34, 12586−12597

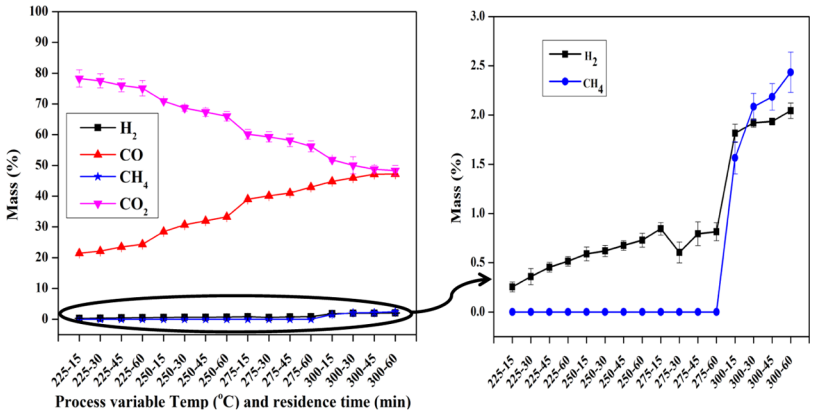

Figure 6. Compositional analyses of gaseous products at different temperatures and retention times during torrefaction.

Table 2. Physical Properties of Liquid Condensates Obtained at Different Torrefaction Temperatures and 30 min Retention Time

properties	TO-225-30	TO-250-30	TO-275-30	TO-300-30
appearance	light brown	light brown	brown	dark brown
HHV (MJ/kg)	10.2	12.5	13.4	14.3
density (kg/m^3)	1052	1063	1072	1086
pH	4.4	3.8	3.2	2.5
carbon residue (wt %)	2.2	2.4	2.9	3.1
ash (wt %)	0.04	0.02	0.01	
viscosity (cP)	0.9	1.6	2.3	3.8
water content (wt %)	65	58	52	45

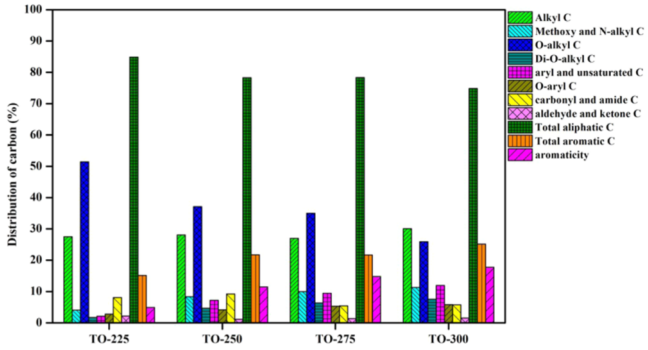

Figure 7. ^{13}C NMR analysis of liquid condensates obtained at different temperatures and 30 min retention time to classify different types of carbon present in the liquid condensate.

respectively, as the temperature varies from 225 to 300 °C. As the torrefaction temperature increases, the viscosity of the liquid condensate decreased due to a decrease in the water content of the liquid condensate. However, the viscosity of TO-300 (3.88 cP) is higher than the viscosity of water, which is found to be 1.00 cP at 20 °C. The pH contents of liquid condensates TO-225-30, TO-250-30, TO-275-30, and TO-300-30 were found to be 4.4, 3.8, 3.2, and 2.5, respectively. The pH content decreased with process temperature, and the pH of TO-300-30 is close to the pH of bio-oil obtained from the pyrolysis of biomass. Ramsbottom carbon residue, which denotes the carbon formation tendency and ash content, varies between 2.2−3.1 and 0.04−0.01 wt %, respectively, once the temperature increased from 225 to 300 °C.

3.4.2. ^{13}C NMR Spectroscopy of Liquid Condensates. The ^{13}C NMR spectroscopy of liquid condensates obtained at different conditions during torrefaction was performed to analyze the types of carbon present in the liquid condensate. The results are shown in Figures 7 and S4. For analysis, the integral spectra of liquid condensate were divided into eight ranges based on chemical shift (Table S1).[56] The integral values of each chemical shift are shown in Figure 7, which indicates the distribution of different types of carbon as a percentage of the total carbon present in the liquid condensate. It was found that alkyl carbon and (methoxyl and N-alkyl carbon) increased from 27.5 to 30.0%, and 4.1 to 11.3%, respectively, while O-alkyl carbon decreased from 51.4 to 25.9%. The total aliphatic carbon decreased from 84.7 to 74.8%. A significant cleavage of the O-alkyl carbon was observed with temperature. The total aromatic carbon increased from 15.1 to 25.1%. The increase in aromatic carbon attributed to an increase in the lignin content of biomass at a higher temperature during torrefaction results in an increase in phenolic compounds in the liquid condensate. The decrease in aliphatic carbon and a relative increase in aromatic carbon result in an increase in aromaticity, which increased from 4.9 to 17.7%. Meanwhile, a slight decrease in carbonyl, amide, aldehyde, and ketone carbon was also noticed, which may be due to an increase in gaseous products such as CO, CH_4, and H_2 at a higher temperature.

3.4.3. GC−MS of Liquid Condensates. The GC−MS analysis was employed for identification of chemical compounds associated with the liquid condensates from torrefaction. The compounds and their relative components of liquid condensate from torrefaction at different conditions are compared in Table S2 and Figure 8. Also, the GC−MS spectra of liquid condensates at different process conditions are shown in Figure S5. The liquid condensates from torrefaction are mainly composed of water and organic compounds such as ketones, aldehydes, alcohols, furan derivatives, and phenol derivatives. However, a small quantity of acid, ester, amines, sugar, and anhydrides was also identified.

The distribution of products such as ketones, alcohol, furan derivatives, and phenolic compounds was highly dependent on the process temperature. In contrast, variation in product distribution for aldehydes and acids was not significant between 225 and 300 °C. The majority of the compounds were identified at higher temperatures (275 and 300 °C), while a few compounds were missing at lower temperatures (225 and 250 °C). The fractions of ketones, alcohol, phenols, furan derivatives, amines, and esters increased with temperature

https://dx.doi.org/10.1021/acs.energyfuels.0c01673
Energy Fuels 2020, 34, 12586−12597

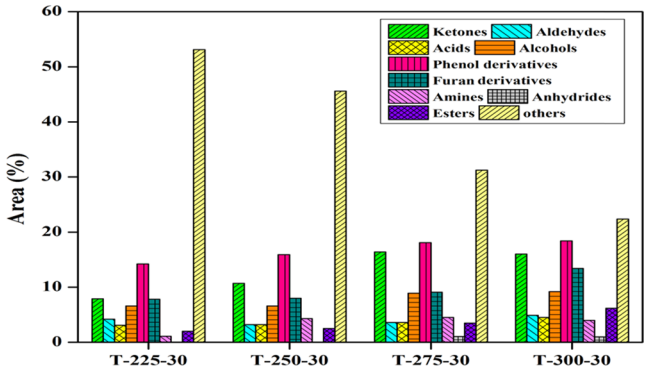

Figure 8. Different classes of chemical compounds and their relative abundance at different temperatures of torrefaction and 30 min retention time.

during torrefaction (Figure 8). The furan derivatives, aldehydes, and ketones are formed from pyranose rings in cellulose by opening of rings and the rearrangement reaction during decomposition of cellulose. Phenol derivative compounds increased with the increase in temperature since at higher temperatures, decomposition of lignin takes place.[40] The yield of 2,5-dimethyl furan (DMF), a platform chemical, may increase between 275 and 300 °C, due to decomposition of the cellulose component of biomass. Li et al.[57] also observed that noncatalytic pyrolysis of cellulose at 300 °C produced furans in appreciable quantities.

3.5. Mechanism of Oxygen Distribution and Carbon Densification during Torrefaction. *3.5.1. Oxygen Distribution and Carbon Densification.* Figure 9a represents the oxygen removal efficiency and carbon densification of biomass during torrefaction. Results showed that the oxygen removal efficiency increased from 14.8 to 39.6% with an increase in temperature from 225 to 300 °C at a retention time of 30 min, while carbon densification increased from 19.6 to 51.8% at similar operating conditions. The distribution of oxygen in the gaseous product is shown in Figure 9b. The oxygen migrated from the raw biomass, mainly in the form of CO_2 and CO. At 225 °C and retention time of 30 min, 77.9% oxygen migrated in the form of CO_2, while 22.0% migrated in the form of CO. At 300 °C and retention time of 30 min, 52.4% oxygen migrated in the form of CO_2, while 47.5% migrated in the form of CO. The distribution of oxygen in liquid condensates is shown in Figure 9c. As per the results obtained from GC−MS analysis of liquid condensates from torrefaction, the oxygen in liquid condensates mainly distributed in the form of water, phenols, acids, furans, ketones, and aldehydes.[26] The dominant oxygen carrier in liquid condensates was water, followed by phenols, ketones, furans, aldehydes, and acids. The distribution of oxygen in water decreased from 63.4 to 43.9%, with an increase in temperature from 225 to 300 °C at a retention time of 30 min, while distribution of oxygen increased in the cases of phenols (from 13.9 to 19.7%), ketones (from 7.7 to 15.6%), furans (from 7.6 to 13.1%), aldehydes (from 4.1 to 4.4%), and acids (from 3.0 to 3.1%).

3.5.2. Mechanism of Oxygen Distribution and Carbon Densification. The fragmentation of different products during thermochemical processes is responsible for the formation of different products. In torrefaction, reactions such as decarboxylation, decarbonylation, and hydration of hemicellulose and cellulose are mainly responsible for the release of CO_2 and CO.[20,34] The cleavage of (C−O−C, −C═O and COOH)

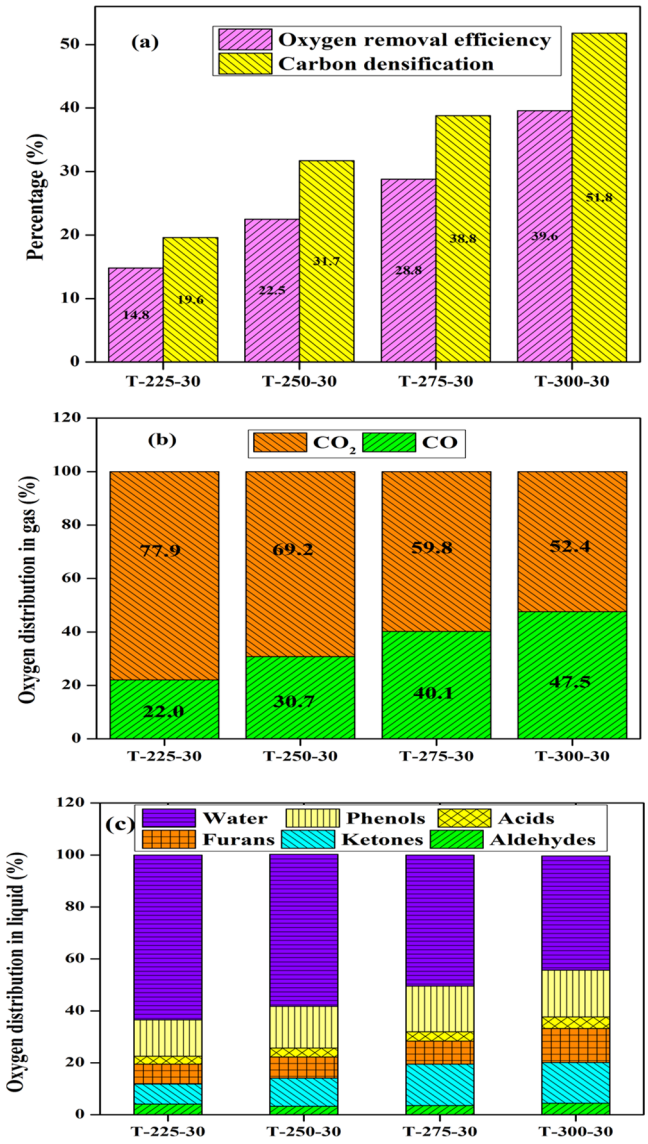

Figure 9. (a) Oxygen removal efficiency and carbon densification, (b) distribution of oxygen in the gaseous product, and (c) distribution of oxygen in the liquid product.

bonds of hemicellulose, cellulose, and lignin led to the formation of CO_2 and CO.[23,31,32] At 225 °C and 60 min retention time, the mass percentages of CO_2 and CO were 75.3 and 24.1%, respectively. While at 300 °C and 60 min retention time, the mass percentages of CO_2 and CO were 49.8 and 46%, respectively. Between CO_2 and CO, decarboxylation mainly favors the formation of CO_2, while decarbonylation mainly favors the formation of CO gas. With an increase in temperature during torrefaction, the amount of CO_2 decreased since the exothermic nature of the decarboxylation reaction inhibits the formation of CO_2 at higher temperatures.[58] The amount of CO increased with an increase in temperature because decarbonylation being endothermic in nature is supported by a high temperature and the amount of CO further increased at higher temperatures.[59] At 225 °C and 60 min retention time, the mass percentage of H_2 was 0.5%, while CH_4 was not detected. At 300 °C and 60 min retention time, the mass percentages of H_2 and CH_4 were 1.9 and 2.0%, respectively. The breaking of methoxyl groups ($-OCH_3$) attached to benzene and the association of alkyl groups to

https://dx.doi.org/10.1021/acs.energyfuels.0c01673
Energy Fuels 2020, 34, 12586−12597

lignin primarily led to H_2 and CH_4 formation.[60] Due to the decomposition of cellulose and hemicellulose, a small fraction of CH_4 was also produced. The furan derivative compounds increased from 7.8 to 13.4% once the temperature increased from 225 to 300 °C at 30 min retention time. The decomposition of hemicellulose mainly yields furan derivative compounds in the liquid condensate.[25] Mainly, decomposition of hemicellulose takes place during torrefaction through the decarboxylation reaction, breaking of glycosidic bonds, fragmentation of inner-ring C−O groups, and C−C bond rupture, which result in the formation of different furan derivative organic compounds.[34] Some furan derivative compounds are also formed through decomposition of cellulose. Cellulose consists of a linear chain of macromolecular polysaccharides, which contains a long chain of glucose. Glucose chains are linked together through β-1,4-glycosidic bonds. These glycosidic bonds are sensitive to acid and thermal treatment.[24] Thus, cleavage of glycosidic bonds mainly contributed to the formation of products from cellulose during thermal treatment. During decomposition of cellulose, aldehydes and ketones are formed from pyranose rings in cellulose through opening of rings and the rearrangement reaction. The ketone derivative compounds increased from 7.9 to 16% once the temperature increased from 225 to 300 °C at 30 min retention time. Lignin consists of complex heteropolymers of phenolic groups, which provides strength to the outer cell wall of plants. Although decomposition of lignin during torrefaction was partial, the phenol derivative compounds containing methoxyl groups were mainly formed from the decomposition of lignin at higher temperatures. The phenol derivative compounds increased from 14.2 to 18.4% once the temperature increased from 225 to 300 °C at 30 min retention time. Phenolic compounds are formed as a result of cleavage of weak α-ether and β-ether bonds associated with lignin. Homolysis and the fragmentation reaction of lignin are mainly responsible for the formation of phenolic compounds. Some simple phenolic compounds were also formed due to the decomposition of hemicellulose. Other compounds like ketones and aldehydes are formed as a result of decomposition of hemicellulose and cellulose via rearrangement and ring-opening reaction of pyranose.[20]

4. CONCLUSIONS

This study reports the experimental investigation of torrefaction of *A. nilotica* at a constant heating rate of 15 °C/min. The ranges of temperature and retention time selected were 225-300 °C and 15−60 min, respectively. The characteristics of the solid residue, liquid condensate, and gaseous products were thoroughly analyzed to increase the understanding of torrefaction based on oxygen distribution and carbon densification. The moisture content decreased by 92.1% and the fixed carbon content increased by 4.2 times of the torrefied biomass (T-300-30) as compared to the raw biomass. Thus, torrefied biomass can be used as a potential feedstock in other thermochemical processes like pyrolysis and gasification. The improvement in characteristics of torrefied biomass as compared to raw biomass was mainly due to oxygen migration and carbon densification in biomass after torrefaction. The oxygen removal efficiency increased from 14.8 to 39.6%, with an increase in temperature from 225 to 300 °C at a retention time of 30 min, while carbon densification increased from 19.6 to 51.8% at similar operating conditions. The migration of oxygen in the gaseous product of torrefaction was mainly in the form of CO_2 and CO, while in the liquid condensate, it mainly distributed in water, phenols, ketones, furans, aldehydes, and acids. In addition, the migration of oxygen was higher, with an increase in temperature during torrefaction at the cost of the yield of the torrefied biomass. The carbon densification in biomass increased with temperature because of an increase in the fixed carbon content (decease in the H/C and O/C ratios) and a decrease in the volatile matter during torrefaction. The composition of liquid condensates and gaseous products varied with temperature. At severe torrefaction conditions, H_2 and CH_4 were also formed, and phenol, furan, and ketone derivative compounds increased, while the water content decreased with temperature.

■ ASSOCIATED CONTENT

Supporting Information

The Supporting Information is available free of charge at https://pubs.acs.org/doi/10.1021/acs.energyfuels.0c01673.

Proximate and ultimate analyses and HHV of raw and torrefied biomass; TGA, FTIR, XRD, GC−MS, and ^{13}C NMR analyses; types of carbon in different ranges of chemical shifts; GC−MS analysis of liquid products; profiles of product yield with variation of temperature; van Krevelan diagram of raw and torrefied biomass (PDF)

■ AUTHOR INFORMATION

Corresponding Author

Jyoti Prasad Chakraborty − *Department of Chemical Engineering and Technology, Indian Institute of Technology (Banaras Hindu University), Varanasi 221005, India;* orcid.org/0000-0001-7914-9358; Phone: +91 979 539 6580; Email: jpc.che@iitbhu.ac.in

Authors

Satyansh Singh − *Department of Chemical Engineering and Technology, Indian Institute of Technology (Banaras Hindu University), Varanasi 221005, India*

Monoj Kumar Mondal − *Department of Chemical Engineering and Technology, Indian Institute of Technology (Banaras Hindu University), Varanasi 221005, India*

Complete contact information is available at: https://pubs.acs.org/10.1021/acs.energyfuels.0c01673

Notes

The authors declare no competing financial interest.

■ ACKNOWLEDGMENTS

The authors acknowledge the funding from the Science and Engineering Research Board (SERB), New Delhi, India, through fund no. SR/FTP/ETA-56/2012. The authors are thankful to Biotech Park Guwahati for carrying out GC−MS analysis. The authors are also grateful to the Department of Chemical Engineering and Technology and Central Instrument Facility Centre (CIFC), Indian Institute of Technology (BHU), Varanasi, for conducting XRD, FTIR, and HHV calculations for the present work.

■ REFERENCES

(1) van der Stelt, M. J. C.; Gerhauser, H.; Kiel, J. H. A.; Ptasinski, K. J. Biomass upgrading by torrefaction for the production of biofuels: A review. *Biomass Bioenergy* **2011**, *35*, 3748−3762.

(2) Dussan, K.; Dooley, S.; Monaghan, R. Integrating compositional features in model compounds for a kinetic mechanism of hemicellulose pyrolysis. *Chem. Eng. J.* **2017**, *328*, 943−961.
(3) Lopez, G.; Alvarez, J.; Amutio, M.; Hooshdaran, B.; Cortazar, M.; Haghshenasfard, M.; Hosseini, S. H.; Olazar, M. Kinetic modeling and experimental validation of biomass fast pyrolysis in a conical spouted bed reactor. *Chem. Eng. J.* **2019**, *373*, 677−686.
(4) Ren, S.; Lei, H.; Zhang, Y.; Wang, L.; Bu, Q.; Wei, Y.; Ruan, R. Furfural production from microwave catalytic torrefaction of Douglas fir sawdust. *J. Anal. Appl. Pyrolysis* **2019**, *138*, 188−195.
(5) Anca-Couce, A.; Obernberger, I. Application of a detailed biomass pyrolysis kinetic scheme to hardwood and softwood torrefaction. *Fuel* **2016**, *167*, 158−167.
(6) Tripathi, M.; Sahu, J. N.; Ganesan, P. Effect of process parameters on production of biochar from biomass waste through pyrolysis: A review. *Renewable Sustainable Energy Rev.* **2016**, *55*, 467−481.
(7) Grams, J.; Kwapińska, M.; Jędrzejczyk, M.; Rzeźnicka, I.; Leahy, J. J.; Ruppert, A. M. Surface characterization of Miscanthus × giganteus and Willow subjected to torrefaction. *J. Anal. Appl. Pyrolysis* **2019**, *138*, 231−241.
(8) Zhou, X.; Li, W.; Mabon, R.; Broadbelt, L. J. A critical review on hemicellulose pyrolysis. *Energy Technol.* **2017**, *5*, 52−79.
(9) Ahmed, A.; Bakar, M. S. A.; Azad, A. K.; Sukri, R. S.; Mahlia, T. M. I. Potential thermochemical conversion of bioenergy from Acacia species in Brunei Darussalam: A review. *Renewable Sustainable Energy Rev.* **2018**, *82*, 3060−3076.
(10) Singh, S.; Chakraborty, J. P.; Mondal, M. K. Torrefaction of woody biomass (*Acacia nilotica*): Investigation of fuel and flow properties to study its suitability as a good quality solid fuel. *Renewable Energy* **2020**, *153*, 711−724.
(11) Huang, Y. W.; Chen, M. Q.; Luo, H. F. Nonisothermal torrefaction kinetics of sewage sludge using the simplified distributed activation energy model. *Chem. Eng. J.* **2016**, *298*, 154−161.
(12) Bach, Q.-V.; Gye, H.-R.; Song, D.; Lee, C.-J. High quality product gas from biomass steam gasification combined with torrefaction and carbon dioxide capture processes. *Int. J. Hydrogen Energy* **2019**, *44*, 14387−14394.
(13) Li, Y.-H.; Chen, H.-H. Analysis of syngas production rate in empty fruit bunch steam gasification with varying control factors. *Int. J. Hydrogen Energy* **2018**, *43*, 667−675.
(14) Sarvaramini, A.; Assima, G. P.; Larachi, F. Dry torrefaction of biomass − Torrefied products and torrefaction kinetics using the distributed activation energy model. *Chem. Eng. J.* **2013**, *229*, 498−507.
(15) Zhao, C.; Qiao, X.; Cao, Y.; Shao, Q. Application of hydrogen peroxide presoaking prior to ammonia fiber expansion pretreatment of energy crops. *Fuel* **2017**, *205*, 184−191.
(16) Cen, K.; Chen, D.; Wang, J.; Cai, Y.; Wang, L. Effects of Water Washing and Torrefaction Pretreatments on Corn Stalk Pyrolysis: Combined Study Using TG-FTIR and a Fixed Bed Reactor. *Energy Fuels* **2016**, *30*, 10627−10634.
(17) Mei, Y.; Che, Q.; Yang, Q.; Draper, C.; Yang, H.; Zhang, S.; Chen, H. Torrefaction of different parts from a corn stalk and its effect on the characterization of products. *Ind. Crops Prod.* **2016**, *92*, 26−33.
(18) Chen, W.-H.; Zhuang, Y.-Q.; Liu, S.-H.; Juang, T.-T.; Tsai, C.-M. Product characteristics from the torrefaction of oil palm fiber pellets in inert and oxidative atmospheres. *Bioresour. Technol.* **2016**, *199*, 367−374.
(19) Chen, W.-H.; Liu, S.-H.; Juang, T.-T.; Tsai, C.-M.; Zhuang, Y.-Q. Characterization of solid and liquid products from bamboo torrefaction. *Appl. Energy* **2015**, *160*, 829−835.
(20) Han, Z.; Zeng, X.; Yao, C.; Xu, G. Oxygen Migration in Torrefaction of Eupatorium adenophorum Spreng. and Its Improvement on Fuel Properties. *Energy Fuels* **2015**, *29*, 7275−7283.
(21) Doddapaneni, T. R. K. C.; Jain, R.; Praveenkumar, R.; Rintala, J.; Romar, H.; Konttinen, J. Adsorption of furfural from torrefaction condensate using torrefied biomass. *Chem. Eng. J.* **2018**, *334*, 558−568.
(22) Demey, H.; Melkior, T.; Chatroux, A.; Attar, K.; Thiery, S.; Miller, H.; Grateau, M.; Sastre, A. M.; Marchand, M. Evaluation of torrefied poplar-biomass as a low-cost sorbent for lead and terbium removal from aqueous solutions and energy co-generation. *Chem. Eng. J.* **2019**, *361*, 839−852.
(23) Yang, H.; Yan, R.; Chen, H.; Lee, D. H.; Zheng, C. Characteristics of hemicellulose, cellulose and lignin pyrolysis. *Fuel* **2007**, *86*, 1781−1788.
(24) Wang, S.; Dai, G.; Yang, H.; Luo, Z. Lignocellulosic biomass pyrolysis mechanism: A state-of-the-art review. *Prog. Energy Combust. Sci.* **2017**, *62*, 33−86.
(25) Demirbaş, A. Mechanisms of liquefaction and pyrolysis reactions of biomass. *Energy Convers. Manage.* **2000**, *41*, 633−646.
(26) Ma, Z.; Zhang, Y.; Shen, Y.; Wang, J.; Yang, Y.; Zhang, W.; Wang, S. Oxygen migration characteristics during bamboo torrefaction process based on the properties of torrefied solid, gaseous, and liquid products. *Biomass Bioenergy* **2019**, *128*, No. 105300.
(27) Singh, S.; Chakraborty, J. P.; Mondal, M. K. Optimization of process parameters for torrefaction of *Acacia nilotica* using response surface methodology and characteristics of torrefied biomass as upgraded fuel. *Energy* **2019**, *186*, No. 115865.
(28) Chen, Y.-H.; Chang, C.-C.; Chang, C.-Y.; Yuan, M.-H.; Ji, D.-R.; Shie, J.-L.; Lee, C.-H.; Chen, Y.-H.; Chang, W.-R.; Yang, T.-Y.; Hsu, T.-C.; Huang, M.; Wu, C.-H.; Lin, F.-C.; Ko, C.-H. Production of a solid bio-fuel from waste bamboo chopsticks by torrefaction for cofiring with coal. *J. Anal. Appl. Pyrolysis* **2017**, *126*, 315−322.
(29) Pachón-Morales, J.; Colin, J.; Pierre, F.; Puel, F.; Perré, P. Effect of torrefaction intensity on the flow properties of lignocellulosic biomass powders. *Biomass Bioenergy* **2019**, *120*, 301−312.
(30) Kanwal, S.; Chaudhry, N.; Munir, S.; Sana, H. Effect of torrefaction conditions on the physicochemical characterization of agricultural waste (sugarcane bagasse). *Waste Manage.* **2019**, *88*, 280−290.
(31) Chen, D.; Gao, A.; Cen, K.; Zhang, J.; Cao, X.; Ma, Z. Investigation of biomass torrefaction based on three major components: Hemicellulose, cellulose, and lignin. *Energy Convers. Manage.* **2018**, *169*, 228−237.
(32) Ma, Z.; Wang, J.; Li, C.; Yang, Y.; Liu, X.; Zhao, C.; Chen, D. New sight on the lignin torrefaction pretreatment: Relevance between the evolution of chemical structure and the properties of torrefied gaseous, liquid, and solid products. *Bioresour. Technol.* **2019**, *288*, No. 121528.
(33) Prins, M. J.; Ptasinski, K. J.; Janssen, F. J. J. G. Torrefaction of wood: Part 2. Analysis of products. *J. Anal. Appl. Pyrolysis* **2006**, *77*, 35−40.
(34) Chen, D.; Gao, A.; Ma, Z.; Fei, D.; Chang, Y.; Shen, C. In-depth study of rice husk torrefaction: Characterization of solid, liquid and gaseous products, oxygen migration and energy yield. *Bioresour. Technol.* **2018**, *253*, 148−153.
(35) Sukiran, M. A.; Abnisa, F.; Daud, W. M. A. W.; Bakar, N. A.; Loh, S. K. A review of torrefaction of oil palm solid wastes for biofuel production. *Energy Convers. Manage.* **2017**, *149*, 101−120.
(36) da Silva, C. M. S.; Carneiro, A. dC. O.; Vital, B. R.; Figueiró, C. G.; de Freitas Fialho, L.; de Magalhães, M. A.; Carvalho, A. G.; Cândido, W. L. Biomass torrefaction for energy purposes−Definitions and an overview of challenges and opportunities in Brazil. *Renewable Sustainable Energy Rev.* **2018**, *82*, 2426−2432.
(37) Dai, G.; Zou, Q.; Wang, S.; Zhao, Y.; Zhu, L.; Huang, Q. Effect of torrefaction on the structure and pyrolysis behavior of lignin. *Energy Fuels* **2018**, *32*, 4160−4166.
(38) Wang, S.; Dai, G.; Ru, B.; Zhao, Y.; Wang, X.; Zhou, J.; Luo, Z.; Cen, K. Effects of torrefaction on hemicellulose structural characteristics and pyrolysis behaviors. *Bioresour. Technol.* **2016**, *218*, 1106−1114.
(39) Wang, S.; Dai, G.; Ru, B.; Zhao, Y.; Wang, X.; Xiao, G.; Luo, Z. Influence of torrefaction on the characteristics and pyrolysis behavior of cellulose. *Energy* **2017**, *120*, 864−871.

https://dx.doi.org/10.1021/acs.energyfuels.0c01673
Energy Fuels 2020, 34, 12586−12597

(40) Chen, D.; Cen, K.; Cao, X.; Li, Y.; Zhang, Y.; Ma, H. Restudy on torrefaction of corn stalk from the point of view of deoxygenation and decarbonization. *J. Anal. Appl. Pyrolysis* **2018**, *135*, 85−93.
(41) Singh, S.; Prasad Chakraborty, J.; Kumar Mondal, M. Intrinsic kinetics, thermodynamic parameters and reaction mechanism of non-isothermal degradation of torrefied *Acacia nilotica* using isoconversional methods. *Fuel* **2020**, *259*, No. 116263.
(42) Singh, S.; Chakraborty, J. P.; Mondal, M. K. Pyrolysis of torrefied biomass: Optimization of process parameters using response surface methodology, characterization, and comparison of properties of pyrolysis oil from raw biomass. *J. Cleaner Prod.* **2020**, *272*, No. 122517.
(43) Bledzki, A. K.; Mamun, A. A.; Volk, J. Physical, chemical and surface properties of wheat husk, rye husk and soft wood and their polypropylene composites. *Composites, Part A* **2010**, *41*, 480−488.
(44) Cai, J.; He, Y.; Yu, X.; Banks, S. W.; Yang, Y.; Zhang, X.; Yu, Y.; Liu, R.; Bridgwater, A. V. Review of physicochemical properties and analytical characterization of lignocellulosic biomass. *Renewable Sustainable Energy Rev.* **2017**, *76*, 309−322.
(45) Lu, Q.; Tian, H.-y.; Hu, B.; Jiang, X.-y.; Dong, C.-q.; Yang, Y.-p. Pyrolysis mechanism of holocellulose-based monosaccharides: The formation of hydroxyacetaldehyde. *J. Anal. Appl. Pyrolysis* **2016**, *120*, 15−26.
(46) Chen, D.; Zhou, J.; Zhang, Q.; Zhu, X.; Lu, Q. Upgrading of Rice Husk by Torrefaction and its Influence on the Fuel Properties. *BioResources* **2014**, *9*, 5893−5905.
(47) Müller-Hagedorn, M.; Bockhorn, H.; Krebs, L.; Müller, U. A comparative kinetic study on the pyrolysis of three different wood species. *J. Anal. Appl. Pyrolysis* **2003**, *68-69*, 231−249.
(48) Chen, Y.-C.; Chen, W.-H.; Lin, B.-J.; Chang, J.-S.; Ong, H. C. Impact of torrefaction on the composition, structure and reactivity of a microalga residue. *Appl. Energy* **2016**, *181*, 110−119.
(49) Min, F.; Zhang, M.; Zhang, Y.; Cao, Y.; Pan, W.-P. An experimental investigation into the gasification reactivity and structure of agricultural waste chars. *J Anal. Appl. Pyrolysis* **2011**, *92*, 250−257.
(50) Azargohar, R.; Nanda, S.; Kozinski, J. A.; Dalai, A. K.; Sutarto, R. Effects of temperature on the physicochemical characteristics of fast pyrolysis bio-chars derived from Canadian waste biomass. *Fuel* **2014**, *125*, 90−100.
(51) Carrasco, F.; Roy, C. Kinetic study of dilute-acid prehydrolysis of xylan-containing biomass. *Wood Sci. Technol.* **1992**, *26*, 189−208.
(52) Gomez-Serrano, V.; Pastor-Villegas, J.; Perez-Florindo, A.; Duran-Valle, C.; Valenzuela-Calahorro, C. FT-IR study of rockrose and of char and activated carbon. *J. Anal. Appl. Pyrolysis* **1996**, *36*, 71−80.
(53) Zheng, A.; Zhao, Z.; Chang, S.; Huang, Z.; Zhao, K.; Wei, G.; He, F.; Li, H. Comparison of the effect of wet and dry torrefaction on chemical structure and pyrolysis behavior of corncobs. *Bioresour. Technol.* **2015**, *176*, 15−22.
(54) Wen, J.-L.; Sun, S.-L.; Yuan, T.-Q.; Xu, F.; Sun, R.-C. Understanding the chemical and structural transformations of lignin macromolecule during torrefaction. *Appl. Energy* **2014**, *121*, 1−9.
(55) Wang, Z.; Cao, J.; Wang, J. Pyrolytic characteristics of pine wood in a slowly heating and gas sweeping fixed-bed reactor. *J. Anal. Appl. Pyrolysis* **2009**, *84*, 179−184.
(56) Zheng, A.; Zhao, Z.; Chang, S.; Huang, Z.; He, F.; Li, H. Effect of Torrefaction Temperature on Product Distribution from Two-Staged Pyrolysis of Biomass. *Energy Fuels* **2012**, *26*, 2968−2974.
(57) Li, W.; Zhu, Y.; Li, S.; Lu, Y.; Wang, J.; Zhu, K.; Chen, J.; Zheng, Y.; Zheng, Z. Catalytic fast pyrolysis of cellulose over Ce0.8Zr0.2-xAlxO2 catalysts to produce aromatic hydrocarbons: Analytical Py-GC × GC/MS. *Fuel Process. Technol.* **2020**, *205*, No. 106438.
(58) Xin, S.; Yang, H.; Chen, Y.; Wang, X.; Chen, H. Assessment of pyrolysis polygeneration of biomass based on major components: Product characterization and elucidation of degradation pathways. *Fuel* **2013**, *113*, 266−273.
(59) Liu, C.; Huang, J.; Huang, X.; Li, H.; Zhang, Z. Theoretical studies on formation mechanisms of CO and CO2 in cellulose pyrolysis. *Comput. Theor. Chem.* **2011**, *964*, 207−212.
(60) Shen, D. K.; Gu, S.; Luo, K. H.; Wang, S. R.; Fang, M. X. The pyrolytic degradation of wood-derived lignin from pulping process. *Bioresour. Technol.* **2010**, *101*, 6136−6146.

https://dx.doi.org/10.1021/acs.energyfuels.0c01673
Energy Fuels 2020, 34, 12586−12597